Photofragment angular momentum distributions in the molecular frame: Determination and interpretation

T. Peter Rakitzis and Richard N. Zare
Department of Chemistry, Stanford University, Stanford, California 94305

(Received 17 September 1998; accepted 11 November 1998)

Photolysis of a molecule typically yields open-shell photofragments having angular momenta. A procedure is described for the measurement of the photofragment angular momentum distribution in terms of polarization parameters $\mathbf{a}_q^{(k)}(p)$ which are expressed in the molecular frame and which may be related to the transition dipole matrix elements. The index (p) indicates either a parallel transition $(\parallel)$, a perpendicular transition $(\perp)$, or a mixed transition $(\parallel,\perp)$ having both parallel and perpendicular character. This procedure has the advantage that it decouples the angular momentum distributions in the molecular frame from the photofragment angular distributions in the laboratory frame, which gives new insight into the photodissociation dynamics. For cases in which $k \leqslant 2$ and with linearly polarized photolysis light, the photofragment angular momentum distribution arising from pure parallel transitions can be described with only one parameter, $\mathbf{a}_0^{(2)}(\parallel)$; photofragment angular momentum distributions arising from pure perpendicular transitions require only two parameters, $\mathbf{a}_0^{(2)}(\perp)$ and $\mathbf{a}_2^{(2)}(\perp)$; photofragment angular momentum distributions arising from mixed transitions, having both parallel and perpendicular character, can be described with five parameters: the two (coherent) interference terms $\mathrm{Im}[\mathbf{a}_1^{(1)}(\parallel,\perp)]$ and $\mathrm{Re}[\mathbf{a}_1^{(2)}(\parallel,\perp)]$ in addition to the three incoherent terms mentioned above. We describe procedures for the measurement of the complete angular momentum distribution of state-selected photofragments using laser detection (such as REMPI) and some form of laboratory velocity selection (such as time-of-flight mass spectrometry, Doppler spectroscopy, or ion imaging). The laser-detection probability of a single photofragment is presented in the form $I=1+f[\theta_\epsilon,\Theta,\Phi,\beta,\mathbf{a}_q^{(k)}(p)]$, where θ_ϵ is the angle between the recoil direction and the photolysis polarization, Θ and Φ are the spherical polar angles describing the orientation of the probe polarization about the recoil direction, and β is the spatial anisotropy parameter. The physical significance of the $\mathbf{a}_q^{(k)}(p)$ is discussed; in particular, the $\mathbf{a}_0^{(k)}(\parallel)$ and $\mathbf{a}_0^{(k)}(\perp)$ describe the photofragment m-state distribution along the recoil direction; the $\mathbf{a}_2^{(k)}(\perp)$ describe how broken cylindrical symmetry in the parent molecule is reflected in the photofragment angular momentum distribution in a plane perpendicular to the recoil direction; and the $\mathbf{a}_1^{(k)}(\parallel,\perp)$ are related to the asymptotic phase difference associated with the interfering channels, and are thus sensitive to the shapes of the dissociative surfaces. © *1999 American Institute of Physics.* [S0021-9606(99)01607-4]

I. INTRODUCTION

The study of vector properties has long been used as a dynamical probe to understand molecular photodissociation. For example, it is well known that the angular distribution of the photofragments, $I(\theta_\epsilon)$, about the polarization of the photodissociating light (for a one-photon photodissociation of an unpolarized sample described by the dipole approximation) is given by[1]

$$I(\theta_\epsilon)=1+\beta P_2(\cos\theta_\epsilon), \tag{1}$$

where θ_ϵ is the angle between the recoil direction and the polarization of the photodissociating light, and P_2 is the second-order Legendre polynomial. The spatial anisotropy parameter β can range from $+2$ for a pure parallel transition $(\Delta\Omega=0)$ to -1 for a pure perpendicular transition $(\Delta\Omega=1)$, when it is assumed that the dissociation is rapid compared to the rotational period of the molecule (axial recoil approximation). Therefore, a measurement of β provides information about the relative symmetry of the dissociating transition. An intermediate value of β indicates that both parallel and perpendicular transitions are being accessed in the axial recoil limit. However, the spatial anisotropy parameter contains little or no information about several aspects of the dissociation dynamics, such as the shape of the dissociating surfaces away from the Franck–Condon region and the nature of curve crossings and other long-range forces that do not alter the asymptotic state of the photofragments. The aim of this paper is to show what can be learned about the photodissociation process from the measurement of photofragment angular momentum vector correlations.

In recent years, there has been considerable experimental and theoretical interest in the angular momentum polarization of photofragments. In 1986 Dixon[2] used a semiclassical treatment to describe the photofragment angular momentum polarization in terms of bipolar moments[3] defined in the laboratory frame, and explained how these parameters can be extracted from the analysis of Doppler-broadened line shapes. Dixon also gave a semiclassical interpretation of the

bipolar moments, which is valid in the high-J limit. Hall and Houston[4] presented in 1989 a review of the determination of vector correlations in photodissociation experiments. A full quantum treatment of the photofragment vector properties has been given by Vasyutinskii[5] in 1983 and by Siebbeles *et al.*[6] in 1994. Recently, Chen and Pei[7] have reexamined the use of photofragment Doppler profiles for determining vector correlations and have developed a full density matrix treatment as an alternative approach.

In this paper we present techniques that show how to measure the complete photofragment angular momentum distribution in the molecular frame. Our treatment uses a formalism that is closely related to that of Siebbeles *et al.* We find that the angular momentum distribution can be described using polarization parameters $\mathbf{a}_q^{(k)}(p)$ discussed in Sec. II, which are similar to the well-known polarization parameters $\mathbf{A}_q^{(k)}$.[8,9] The advantage of working in the molecular frame is as follows: the $\mathbf{a}_q^{(k)}(p)$ decouple the dynamical features of the angular momentum distribution in the molecular frame from laboratory vector correlations and frame transformations. For example, if the spatial anisotropy parameter varies with photolysis wavelength, even if the dynamical features of the angular momentum distribution do not change (i.e., the $\mathbf{a}_q^{(k)}(p)$ are constant), then the laboratory frame angular momentum distributions can change significantly. This variation can obscure the true nature of dynamical effects in photodissociation. Furthermore, each $\mathbf{a}_q^{(k)}(p)$ parameter possesses separate physical significance. The $\mathbf{a}_q^{(k)}(p)$ are classified as $\mathbf{a}_q^{(k)}(\parallel)$, $\mathbf{a}_q^{(k)}(\perp)$, and $\mathbf{a}_q^{(k)}(\parallel,\perp)$. The $\mathbf{a}_q^{(k)}(\parallel)$ parameters are the contributions from the parallel transitions to the photofragment angular momentum distribution, the $\mathbf{a}_q^{(k)}(\perp)$ parameters are the contributions from the perpendicular transitions, and the $\mathbf{a}_q^{(k)}(\parallel,\perp)$ parameters are the contributions from the interference between the parallel and perpendicular transitions. As such, the $\mathbf{a}_q^{(k)}(\parallel)$ and $\mathbf{a}_q^{(k)}(\perp)$ are *incoherent* contributions, and the $\mathbf{a}_q^{(k)}(\parallel,\perp)$ are *coherent* contributions.

The power of the $\mathbf{a}_q^{(k)}(p)$ formalism has been demonstrated in the observation of mass-dependent polarization of the Cl-atom angular momentum in the photolysis of ICl in this laboratory.[10,11] It was shown that the large differences in the alignment of the ^{35}Cl and the ^{37}Cl atoms arise solely from the interference of two dissociating states, expressed in the angular momentum distribution through the $\mathrm{Re}[\mathbf{a}_1^{(2)}(\parallel,\perp)]$ parameter.[10] Additionally, it was shown that the measurement of photofragment orientation, the $\mathrm{Im}[\mathbf{a}_1^{(1)}(\parallel,\perp)]$ parameter, as a function of photodissociation wavelength is sensitive to the phase difference between the dissociating channels, and hence sensitive to the shapes of the dissociative surfaces.[11] Finally, the complete $\mathbf{a}_q^{(k)}(p)$ formalism using linearly polarized photolysis light is illustrated in the experimental study of the photodissociation of ICl and Cl_2 in the companion paper.[12]

In Sec. II, the photofragment angular momentum distribution is described in terms of the molecular frame parameters $\mathbf{a}_q^{(k)}(p)$. Section III presents the molecular frame detection probability in terms of the $\mathbf{a}_q^{(k)}(p)$ and the angles between the recoil direction and the photolysis and probe polarization directions. In Sec. IV the dependence of experimental signals on the $\mathbf{a}_q^{(k)}(p)$ is shown. Section V provides physical interpretation for the $\mathbf{a}_q^{(k)}(p)$. An Appendix presents the connection between the $\mathbf{a}_q^{(k)}(p)$ and the transition dipole matrix elements, and describes the use of circularly polarized photolysis light.

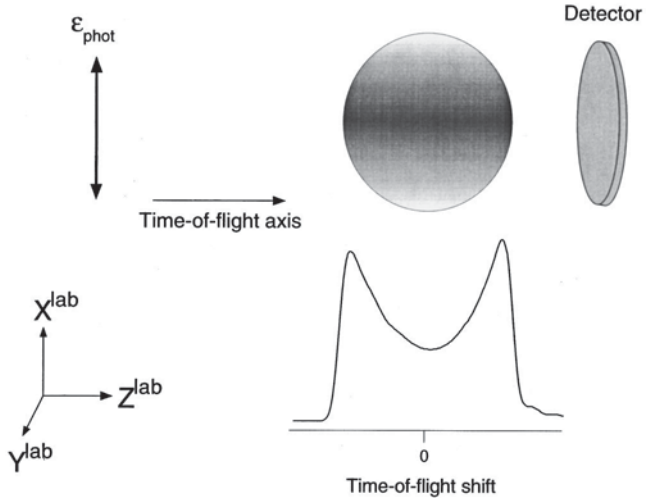

FIG. 1. Ion-arrival profile for a monoenergetic speed distribution for which the ionization probability is independent of the photofragment polarization.

II. PHOTOFRAGMENT ANGULAR MOMENTUM DISTRIBUTIONS

The monoenergetic photofragment velocity distribution resulting from the photolysis of stationary molecules AB is described by Eq. (1); it can be thought of as a shell in velocity space with a surface density that is cylindrically symmetric with respect to the photolysis polarization (see Fig. 1). A more complicated velocity distribution can be described by an appropriate sum of such shells. This velocity distribution can be measured with techniques such as time-of-flight mass spectroscopy, Doppler spectroscopy, and ion imaging. Figure 1 shows the time-of-flight profile of a monoenergetic velocity distribution. This profile is fit with the output of a Monte Carlo simulation. The advantage of simulating the profiles is that the effects of (molecular frame) photofragment polarization on the detection efficiency can be treated for each individual photofragment; in addition to the simulation, all that must be known is the relative laser-detection probability of each photofragment as a function of its polarization and the directions of the photolysis and probe polarizations. In this paper, we will present this laser-detection probability in the form:

$$I = 1 + f[\theta_\epsilon, \Theta, \Phi, \beta, \mathbf{a}_q^{(k)}(p)], \tag{2}$$

where the angles θ_ϵ, Θ, and Φ describe the orientation of the photofragment's laboratory velocity with respect to the photolysis and probe laser polarizations. The detection probability of each individual photofragment in the Monte Carlo simulation is modified with the use of Eq. (2). This approach has been used by Rakitzis *et al.*[13] for the description of product rotational polarization from bimolecular reactions.

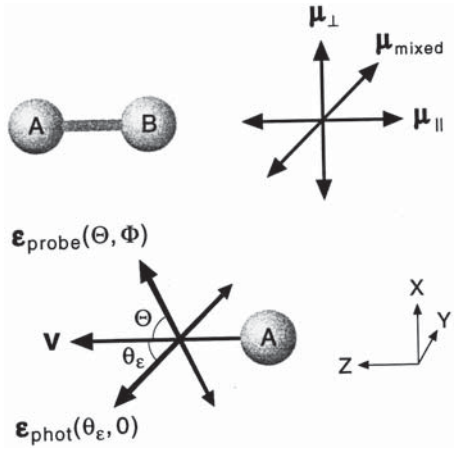

FIG. 2. Molecular frame. The z axis is parallel to $\mathbf{v}$, and the y axis is perpendicular to the plane defined by $\mathbf{v}$ and the photolysis polarization axis ϵ_{phot}. The angle between $\mathbf{v}$ and ϵ_{phot} is θ_ϵ, the angle between $\mathbf{v}$ and ϵ_{probe} is Θ, and Φ is the azimuthal angle of ϵ_{phot} and ϵ_{probe} about $\mathbf{v}$.

In this paper, we shall describe the photofragment polarization in the molecular frame using linearly polarized photolysis light. In this frame, the z axis is given by the photofragment recoil direction $\hat{\mathbf{v}}$ and the y axis is perpendicular to the plane defined by the photolysis polarization and the photofragment velocity ($\hat{y}=\hat{\boldsymbol{\epsilon}}_{\text{phot}}\times\hat{\mathbf{v}}$). Figure 2 shows the right-handed molecular-frame coordinate system and the relevant angles θ_ϵ, Θ, and Φ.

The spatial distribution $D(\theta,\varphi)$ of an ensemble of angular momenta $\mathbf{J}$ can be described by an expansion in modified spherical harmonics. The coefficients or moments of this expansion are the well-known polarization parameters $\mathbf{A}_q^{(k)}$:[9]

$$D(\theta,\varphi)=\sum_{k=0}^{2J}\sum_{q=-k}^{k}\mathbf{A}_q^{(k)}C_q^k(\theta,\varphi), \tag{3}$$

where θ and φ are spherical polar angles in the molecular frame, and the $C_q^k(\theta,\varphi)$ are modified spherical harmonics: $C_q^k(\theta,\varphi)=(4\pi/2k+1)^{1/2}Y_{kq}(\theta,\varphi)$. Equation (3) can be used to describe the photofragment angular momentum distribution in the molecular frame for a fixed angle θ_ϵ (between $\hat{\boldsymbol{\epsilon}}_{\text{phot}}$ and $\hat{\mathbf{v}}$; see Fig. 2). However, in general, the $\mathbf{A}_q^{(k)}$ depend explicitly on θ_ϵ. Therefore, the $(2J+1)^2$ polarization parameters from Eq. (3) are not sufficient to describe the photofragment angular momentum distribution for arbitrary values of θ_ϵ. In this paper we show that Eq. (3) can be used for the description of the angular momentum distributions arising from pure parallel or pure perpendicular transitions (for arbitrary values of θ_ϵ), and we show how the complete description of photofragment angular momentum distributions can be built up from considering the incoherent and coherent contributions from these parallel and perpendicular transitions.

Here, we shall introduce a very similar set of parameters, the $\mathbf{a}_q^{(k)}(p)$, which allow us to express the photofragment angular momentum distribution in the molecular frame for arbitrary values of θ_ϵ in a form similar to Eq. (3):

$$D(\theta,\varphi)=\sum_{k=0}^{2J}\sum_{q=-2}^{2}\sum_{p}\mathbf{a}_q^{(k)}(p)F_q^k(\theta_\epsilon,\beta;p)C_q^k(\theta,\varphi). \tag{4}$$

Notice that in each term of this expansion, there is a complete separation of the angles describing the molecular frame angular momentum distribution (θ and φ) from the variables involved in the laboratory-frame transformations (θ_ϵ and β). In the molecular frame, the one-photon excitation process limits $|q|\leqslant 2$. Notice also that there is an additional summation over the index p. When $q=0$, p can be ($\parallel$) or ($\perp$); when $|q|=1$, p is given by ($\parallel$,$\perp$) only; when $|q|=2$, p is given by ($\perp$) only. Using this notation, the $\mathbf{a}_q^{(k)}(p)$ are classified as $\mathbf{a}_q^{(k)}(\parallel)$, $\mathbf{a}_q^{(k)}(\perp)$, and $\mathbf{a}_q^{(k)}(\parallel,\perp)$. The $\mathbf{a}_q^{(k)}(\parallel)$ describe the polarization of photofragments from parallel transitions only, the $\mathbf{a}_q^{(k)}(\perp)$ describe the polarization of photofragments from perpendicular transitions only, and the $\mathbf{a}_q^{(k)}(\parallel,\perp)$ represent contributions to the photofragment polarization that arise from the interference between parallel and perpendicular transitions. As will be seen, the set of parameters $\mathbf{a}_q^{(k)}(\parallel)$, $\mathbf{a}_q^{(k)}(\perp)$, and $\mathbf{a}_q^{(k)}(\parallel,\perp)$ represent a very physical and intuitive picture of the photodissociation dynamics. For linearly polarized light, the maximum number of $\mathbf{a}_q^{(k)}(p)$ parameters in the molecular frame reduces to $5J$ for integer J and $5J$-3/2 for half-integer J.

For a pure parallel transition, both the transition dipole moment μ and the bond axis are parallel to the recoil direction; thus there is only one physically significant axis. Cylindrical symmetry of the parent molecules ensures that the photofragment angular momentum distributions must also possess cylindrical symmetry. This symmetry constrains all noncylindrically symmetric parameters (with $q\neq 0$) to vanish [i.e., $\mathbf{a}_q^{(k)}(\parallel)=0$ for $q\neq 0$]. Because μ is always parallel to $\hat{\mathbf{v}}$, the photofragment angular momentum distribution will not depend on θ_ϵ. Additionally, for a parallel transition, there is no net change in the projection of the total angular momentum onto the bond axis ($\Delta\Omega=0$) so that the ensemble of parent molecules possess no net orientation. Thus, for the photolysis of molecules AB through a parallel transition, the $\mathbf{a}_0^{(k)}(\parallel)$ for the photofragments A and B must vanish for odd k. These constraints allow Eq. (3) to be recast to give the photofragment angular momentum distribution $D_\parallel(\theta)$ arising from a pure parallel transition:

$$D_\parallel(\theta)=\sum_{k=0}^{2J}\mathbf{a}_0^{(k)}(\parallel)C_0^k(\theta,\varphi), \tag{5}$$

where Eq. (5) is identical to Eq. (3) except that q is constrained to be 0 and k to be even.

In many instances, we only need to be concerned with $k\leqslant 2$. The polarization of ensembles of $J\leqslant 1$ are fully described with $k\leqslant 2$ only. Additionally, if the photofragments are probed via a one-photon absorption process, then the detection process is only sensitive to the parameters with $k\leqslant 2$ for any value of J. To illustrate these common cases, Eq. (5) becomes for $k\leqslant 2$:

$$D_\parallel(\theta)=1+\mathbf{a}_0^{(2)}(\parallel)P_2(\cos\theta). \tag{6}$$

For a pure perpendicular transition, the transition dipole moment μ is perpendicular to the bond axis. Reflection symmetry through planes defined by $\hat{\mathbf{v}}$ and μ, and by $\hat{\mathbf{v}}$ and $\mu \times \hat{\mathbf{v}}$, ensures that parameters with odd q vanish. The spatial distribution $D_\perp(\theta,\varphi)$ of the angular momenta $\mathbf{J}$ of an ensemble of photofragments from a pure perpendicular transition is given by

$$D_\perp(\theta,\varphi)=\sum_{k=0}^{2J}\sum_{q=-2}^{2}\mathbf{a}_q^{(k)}(\perp)C_q^k(\theta,\varphi) \quad (|q|\neq 1), \tag{7}$$

where Eq. (7) is identical to Eq. (3) except that q is constrained to be 2, 0 and -2 only and k to be even; the nature of the one-photon photodissociation process restricts $|q| \leqslant 2$, and the symmetry of perpendicular transitions constrains parameters with $|q|=1$ to be zero. The use of linearly polarized photolysis light constrains k to be even for perpendicular transitions, but in contrast to pure parallel transitions, the $\mathbf{a}_0^{(k)}(\perp)$ and $\mathbf{a}_2^{(k)}(\perp)$ orientation parameters with odd k can be present when the photolysis light is circularly polarized (see Appendix). For $k\leqslant 2$, Eq. (7) becomes

$$D_\perp(\theta,\varphi) = 1+\mathbf{a}_0^{(2)}(\perp)P_2(\cos\theta)+\mathbf{a}_2^{(2)}(\perp)\sqrt{3/2}\sin^2\theta\cos 2\varphi. \tag{8}$$

Notice that because $\mathbf{a}_q^{(k)}(p)=(-1)^q\mathbf{a}_{-q}^{(k)}(p)^*$, the $q=-2$ term is expressed in terms of the $q=2$ term [in particular, since $\mathbf{a}_2^{(2)}(\perp)$ is real, $\mathbf{a}_{-2}^{(2)}(\perp)=\mathbf{a}_2^{(2)}(\perp)$].

A mixed transition is one in which both parallel and perpendicular components are accessed, so that μ is neither parallel nor perpendicular to the bond axis, as shown in Fig. 2. This symmetry breaking allows the existence of the $\mathrm{Re}[\mathbf{a}_1^{(k)}(\parallel,\perp)]$ with even k and the $\mathrm{Im}[\mathbf{a}_1^{(k)}(\parallel,\perp)]$ with odd k (whereas the $\mathrm{Im}[\mathbf{a}_1^{(k)}(\parallel,\perp)]$ with even k and the $\mathrm{Re}[\mathbf{a}_1^{(k)}(\parallel,\perp)]$ with odd k can only be observed with circularly polarized photolysis light; see Appendix). Kupriyanov and Vasyutinskii[14] and Siebbeles *et al.*[6] have shown that the interference between parallel and perpendicular transitions is solely expressed by the $|q|=1$ terms (in a one-photon dissociation process). We can now construct the mixed-transition photofragment angular momentum distribution, $D_{\parallel,\perp}$, as a normalized weighted sum of the incoherent contributions from parallel and perpendicular transitions [given by Eqs. (5) and (7)] as well as the addition of the $|q|=1$ interference terms:

$$D_{\parallel,\perp}(\theta_\epsilon,\beta,\theta,\varphi) = \Big[(1+\beta)\cos^2\theta_\epsilon D_\parallel(\theta)+(1-\beta/2)\sin^2\theta_\epsilon D_\perp(\theta,\varphi) + 2\sin\theta_\epsilon\cos\theta_\epsilon\sum_{k=0}^{2J}\mathbf{a}_1^{(k)}(\parallel,\perp)C_1^k(\theta,\varphi)\Big] \Big/ [1+\beta P_2(\cos\theta_\epsilon)]. \tag{9}$$

Unlike either Eq. (5) or Eq. (7), $D_{\parallel,\perp}$ depends explicitly on θ_ϵ and β. The terms $(1+\beta)\cos^2\theta_\epsilon$, $(1-\beta/2)\sin^2\theta_\epsilon$, and $2\sin\theta_\epsilon\cos\theta_\epsilon$ [all divided by the normalization factor $1+\beta P_2(\cos\theta_\epsilon)$] are the weighting factors for the incoherent and coherent contributions. Notice that a more appropriate weighting factor for the cross term would be $2\sqrt{(1+\beta)(1-\beta/2)}\sin\theta_\epsilon\cos\theta_\epsilon$, which is twice the product of the square roots of the incoherent contributions, as expected. However, the factor $\sqrt{(1+\beta)(1-\beta/2)}$ is extremely sensitive to the value of β close to the limiting values of $+2$ and -1. Because with current techniques β cannot be measured to the necessary accuracy of about 1%, we decided to define the $\mathbf{a}_1^{(k)}(\parallel,\perp)$ terms so as to incorporate the factor of $\sqrt{(1+\beta)(1-\beta/2)}$. Thus, the interference terms vanish for the limiting cases of $\beta=+2$ or -1, as expected. Notice that for $\beta=+2$, $D_{\parallel,\perp}(\theta_\epsilon,\beta,\theta,\varphi)$ reduces to $D_\parallel(\theta)$, whereas for $\beta=-1$, $D_{\parallel,\perp}(\theta_\epsilon,\beta,\theta,\varphi)$ reduces to $D_\perp(\theta,\varphi)$. Even when β is close to $+2$ or -1, and the incoherent contributions from one channel are small, the magnitude of the interference terms can be quite large. For example, for the case of $\beta=+1.8$, the term $\sqrt{(1+\beta)(1-\beta/2)}$ is reduced to only 50% of its maximal value, whereas for the nearly pure parallel case of $\beta=+1.99$ the interference contribution is reduced to only 12% of its maximal value! Therefore, the $|q|=1$ interference terms are extremely sensitive to the mixing of states of parallel and perpendicular symmetry.

Equation (9), unlike Eqs. (5) and (7), is no longer of the form of Eq. (3); therefore, for a mixed transition, the parameters used to describe the photofragment angular momentum distribution, the $\mathbf{a}_q^{(k)}(p)$, no longer follow the standard polarization parameter definition of the $\mathbf{A}_q^{(k)}$. However, as we have seen, the $\mathbf{a}_q^{(k)}(\parallel)$ and $\mathbf{a}_q^{(k)}(\perp)$ are the standard polarization parameters for pure parallel and perpendicular transitions respectively, whereas the $\mathbf{a}_q^{(k)}(\parallel,\perp)$ parameters result from the interference of parallel and perpendicular transitions. Most importantly, the $\mathbf{a}_q^{(k)}(p)$ transform under rotation as the $\mathbf{A}_q^{(k)}$. By recasting Eq. (9) in the form of Eq. (3), we find that the molecular-frame polarization parameters $\mathbf{A}_q^{(k)}$ are given by

$$\mathbf{A}_0^{(k)}=[(1+\beta)\cos^2\theta_\epsilon\mathbf{a}_0^{(k)}(\parallel)+(1-\beta/2)\sin^2\theta_\epsilon\mathbf{a}_0^{(k)}(\perp)]/[1+\beta P_2(\cos\theta_\epsilon)], \tag{10}$$

$$\mathbf{A}_1^{(k)}=\sin\theta_\epsilon\cos\theta_\epsilon\mathbf{a}_1^{(k)}(\parallel,\perp)/[1+\beta P_2(\cos\theta_\epsilon)], \tag{11}$$

$$\mathbf{A}_2^{(k)}=(1-\beta/2)\sin^2\theta_\epsilon\mathbf{a}_2^{(k)}(\perp)/[1+\beta P_2(\cos\theta_\epsilon)], \tag{12}$$

where

$$\mathbf{A}_q^{(k)}=(-1)^q\mathbf{A}_{-q}^{(k)*}. \tag{13}$$

These equations give the explicit dependence of the $\mathbf{A}_q^{(k)}$ on θ_ϵ, β, and the $\mathbf{a}_q^{(k)}(p)$, and allow us to subsequently derive the photofragment detection probability $I=1+f[\theta_\epsilon,\Theta,\Phi,\beta,\mathbf{a}_q^{(k)}(p)]$ as a function of the molecular-frame polarization and the laboratory detection geometry. Explicitly, the molecular-frame angular momentum distribution in terms of the $\mathbf{a}_q^{(k)}(p)$ for $k\leqslant 2$ is given by

$$\begin{aligned}D_{\parallel,\perp}(\theta,\varphi,\theta_\epsilon,\beta) = 1+\{&\sin\theta_\epsilon\cos\theta_\epsilon\,\mathrm{Im}[\mathbf{a}_1^{(1)}(\parallel,\perp)]\sqrt{2}\sin\theta\sin\varphi \\ &+(1+\beta)\cos^2\theta_\epsilon\mathbf{a}_0^{(2)}(\parallel)P_2(\cos\theta) \quad +(1-\beta/2) \\ &\times\sin^2\theta_\epsilon\mathbf{a}_0^{(2)}(\perp)P_2(\cos\theta)+\sin\theta_\epsilon\cos\theta_\epsilon \\ &\times\mathrm{Re}[\mathbf{a}_1^{(2)}(\parallel,\perp)]\sqrt{3/2}\sin 2\theta\cos\varphi+(1-\beta/2)\sin^2\theta_\epsilon \\ &\times\mathbf{a}_2^{(2)}(\perp)\sqrt{3/2}\sin^2\theta\cos 2\varphi\}/[1+\beta P_2(\cos\theta_\epsilon)].\end{aligned} \tag{14}$$

For many practical cases, Eq. (14) is the major result of this paper. It shows that in the most general case the angular momentum distribution can be represented by the population [which is normalized to unity in our treatment and is the first term on the right side of Eq. (14)], one orientation parameter {the $\mathrm{Im}[\mathbf{a}_1^{(1)}(\parallel,\perp)]$}, four alignment parameters [the $\mathbf{a}_0^{(2)}(\parallel)$, $\mathbf{a}_0^{(2)}(\perp)$, $\mathrm{Re}[\mathbf{a}_1^{(2)}(\parallel,\perp)]$, and $\mathbf{a}_2^{(2)}(\perp)$], and the spatial anisotropy parameter (β), which makes a total of seven parameters.

III. DETECTION PROBABILITY

The relative detection probability of an atom or molecule using REMPI or LIF (in which the emitted photon is detected independent of its polarization) with polarized light can be expressed in terms of the polarization parameters in a simple form:[3,15]

$$I(\Theta,\Phi,A_q^{(k)})=\sum_{k=0}^{2n}\sum_{q=-k}^{k} s_k \mathbf{A}_q^{(k)} C_q^k(\Theta,\Phi), \tag{15}$$

where the laser-detection sensitivity s_k depends on the details of spectral transition of the resonant step, such as the quantum numbers of the ground state and the resonant state, and the degree of ellipticity of the light involved in the detection process. General methods for calculating parameters similar to the s_k for $(2+1)$ REMPI and LIF for atoms, diatomic, and symmetric-top molecules are reported by Kummel *et al.*;[15,16] Rakitzis *et al.*[13] give expressions for the s_k in terms of the notation of Kummel *et al.* Simple techniques are given in the following paper[12] to calculate the s_k for special cases when J is small. Also, Θ is the angle between the detection axis (in this case the recoil direction $\hat{\mathbf{v}}$) and the polarization axis $\boldsymbol{\epsilon}_{\mathrm{probe}}$ of the detection laser beam; Φ is the angle between the projections of $\boldsymbol{\epsilon}_{\mathrm{probe}}$ and $\boldsymbol{\epsilon}_{\mathrm{phot}}$ onto the plane perpendicular to the detection axis; and n is the number of photons in the resonant step of the $(n+m)$ REMPI or LIF process. For the REMPI process, the ionization step is assumed to be saturated, whereas for the LIF process the emitted photons are assumed to be detected independent of their polarization. The general detection expression of Eq. (15) can be combined with the photofragment polarization parameters of Eqs. (10)–(13) to give a complete description of the photofragment detection probability in the molecular frame; this expression is given explicitly for parameters of $k\leqslant 2$:

$$\begin{aligned} I[\Theta,\Phi,\theta_\epsilon,\beta,\mathbf{a}_q^{(k)}(p)] &= 1+(s_1\sin\theta_\epsilon\cos\theta_\epsilon\,\mathrm{Im}[\mathbf{a}_1^{(1)}(\parallel,\perp)]\sqrt{2}\sin\Theta\sin\Phi \\ &+ s_2\{(1+\beta)\cos^2\theta_\epsilon \mathbf{a}_0^{(2)}(\parallel)P_2(\cos\Theta)+(1-\beta/2) \\ &\times\sin^2\theta_\epsilon \mathbf{a}_0^{(2)}(\perp)P_2(\cos\Theta)+\sin\theta_\epsilon\cos\theta_\epsilon \\ &\times\mathrm{Re}[\mathbf{a}_1^{(2)}(\parallel,\perp)]\sqrt{3/2}\sin 2\Theta\cos\Phi+(1-\beta/2)\sin^2\theta_\epsilon \\ &\times\mathbf{a}_2^{(2)}(\perp)\sqrt{3/2}\sin^2\Theta\cos 2\Phi\})/[1+\beta P_2(\cos\theta_\epsilon)]. \end{aligned} \tag{16}$$

Equation (16) is the central result of this article. This equation relates laser-detection probability, the laboratory observable, to the $\mathbf{a}_q^{(k)}(p)$ that describe the angular momentum distribution in the molecular frame. Section IV describes the use of this equation to generate basis functions for the analysis of experimental profiles.

For a pure parallel transition when β is equal to $+2$, Eq. (16) reduces to

$$I[\Theta,\mathbf{a}_q^{(k)}(\parallel)]=1+s_2\mathbf{a}_0^{(2)}(\parallel)P_2(\cos\Theta). \tag{17}$$

Notice that the detection probability has no explicit dependence on the photolysis polarization direction. For a pure perpendicular transition when β is equal to -1, Eq. (16) reduces to

$$\begin{aligned} I[\Theta,\Phi,\mathbf{a}_q^{(k)}(\perp)] &= 1+s_2[\mathbf{a}_0^{(2)}(\perp)P_2(\cos\Theta) \\ &+\mathbf{a}_2^{(2)}(\perp)\sqrt{3/2}\sin^2\Theta\cos 2\Phi]. \end{aligned} \tag{18}$$

Notice that, again, the detection probability has no explicit dependence on the angle θ_ϵ between the photolysis polarization direction and the recoil direction; however, the projection of the photolysis polarization direction onto the plane perpendicular to the recoil direction is used in the determination of Φ. As mentioned earlier, Eqs. (17) and (18) should be used only if there is no mixed-state contribution.

IV. POLARIZATION-DEPENDENT BASIS FUNCTIONS

As shown in the previous section, the experimental sensitivity to the $\mathbf{a}_q^{(k)}(p)$ depends on the spatial anisotropy parameter β. Furthermore, if β is known, then the anisotropic experimental signals (described below) depend linearly on the $\mathbf{a}_q^{(k)}(p)$; hence a previous measurement of β greatly facilitates the subsequent measurement of the $\mathbf{a}_q^{(k)}(p)$. In order to decouple the measurement of β from the effects of the $\mathbf{a}_q^{(k)}(p)$, the photofragments must be detected on a spectral branch that is insensitive to photofragment polarization, or experimental profiles can be summed to remove the effects of the $\mathbf{a}_q^{(k)}(p)$; for parameters with $k=2$ this is achieved by summing profiles in which the probe polarization lies along three orthogonal axes. Additionally, in some circumstances, the effects of the of the $\mathbf{a}_q^{(k)}(p)$ on the measurement of β can be neglected owing to their reduction from strong hyperfine depolarization effects.[17] Once profiles are obtained that are independent of photofragment polarization, then the photofragment population and spatial anisotropy can be measured. Methods for measuring the spatial anisotropy are described elsewhere.[18]

The creation of polarization-dependent basis functions used to fit experimental signals from product polarization in bimolecular reactions has been given previously;[13] a similar basis-function method is described here. The brief description given here uses examples involving time-of-flight mass spectrometry, although the methods described here are completely general for any other velocity-sensitive detection technique, such as Doppler spectroscopy and ion imaging. The spatial distribution of photofragments, and their subsequent velocity-dependent detection, is modeled with a Monte Carlo simulation (see Fig. 1). Up to this point, the laser-detection probability as a function of photofragment polarization is assumed to be unity for all photofragments [from

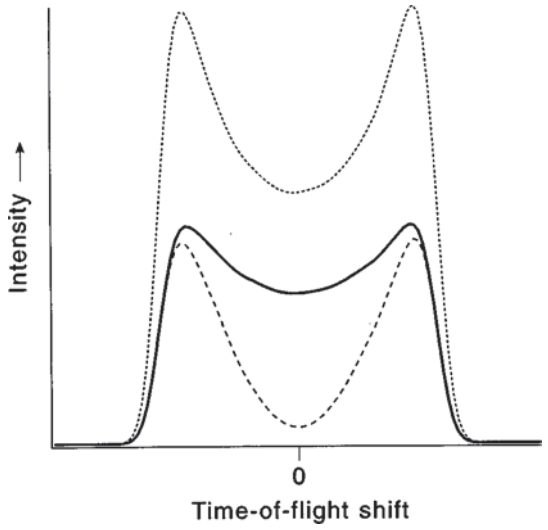

FIG. 3. Single-speed ion-arrival basis functions for the photodissociation of ICl that demonstrate the effect of the $\mathbf{a}_2^{(2)}(\perp)$ and the position of the probe polarization on polarization-dependent basis functions: The $\mathbf{B}_{\rm iso}^X[t]$ time-of-flight profile (solid line) simulates monoenergetic photofragments with $\beta=-0.6$, the photolysis polarization along the X axis and exhibiting no photofragment polarization effects [all $\mathbf{a}_q^{(k)}(p)=0$]. The profile $\mathbf{B}_X^X[\mathbf{a}_2^{(2)}(\perp);t]$ (dotted line) simulates the effect of a value of $\mathbf{a}_2^{(2)}(\perp)=1$ on the experimental profile with the probe polarization parallel to the X axis, whereas the $\mathbf{B}_Z^X[\mathbf{a}_2^{(2)}(\perp);t]$ profile (dashed line) simulates the same effect but with the probe polarization parallel to the Z axis.

Eq. (2), $I=1$]. Figure 3 shows the time-of-flight profile $\mathbf{B}_{\rm iso}^X$ for a mixed transition with $\beta=-0.6$. The superscript X indicates that the photolysis polarization $\hat{\boldsymbol{\epsilon}}_{\rm phot}$ lies along the laboratory X axis (see Fig. 1 for the definition of the laboratory axis), and the subscript iso indicates that the photofragment polarization is isotropic, so that the photofragment polarization does not effect the experimental signals. The other two profiles are discussed below.

To include the effect of photofragment polarization on the modeling of the experimental signals, the total detection probability of each photofragment is multiplied by the polarization-dependent laser-detection probability given by Eq. (16). For example, consider photofragments characterized by $\beta=-0.6$, $\mathbf{a}_2^{(2)}(\perp)=+1$, and all other $\mathbf{a}_q^{(k)}(p)=0$, detected via a spectral transition characterized by $s_2=1$. In this case, the laser-detection probability of Eq. (16) reduces to

$$I[\Theta,\Phi,\theta_\epsilon]=1+[1.3\sin^2\theta_\epsilon\sqrt{3/2}\sin^2\Theta\cos 2\Phi]/[1-0.6P_2(\cos\theta_\epsilon)]. \tag{19}$$

For each individual photofragment in the simulation, the total detection probability is multiplied by Eq. (19). For laboratory unit vectors $\hat{\boldsymbol{\epsilon}}_{\rm probe}$ and $\hat{\boldsymbol{\epsilon}}_{\rm phot}$, and for each photofragment recoil velocity unit vector $\hat{\mathbf{v}}$, the angles θ_ϵ, Θ, and Φ are given by

$$\cos\theta_\epsilon=\hat{\boldsymbol{\epsilon}}_{\rm phot}\cdot\hat{\mathbf{v}}, \tag{20}$$

$$\cos\Theta=\hat{\boldsymbol{\epsilon}}_{\rm probe}\cdot\hat{\mathbf{v}}, \tag{21}$$

$$\cos\Phi=\frac{\mathbf{P}_{\rm phot}\cdot\mathbf{P}_{\rm probe}}{|\mathbf{P}_{\rm phot}||\mathbf{P}_{\rm probe}|}, \tag{22}$$

where $\mathbf{P}_{\rm phot}$ is the projection of $\hat{\boldsymbol{\epsilon}}_{\rm phot}$ onto the plane perpendicular to $\hat{\mathbf{v}}$ and is given by

$$\mathbf{P}_{\rm phot}=\hat{\boldsymbol{\epsilon}}_{\rm phot}-\cos\theta_\epsilon\hat{\mathbf{v}}, \tag{23}$$

and $\mathbf{P}_{\rm probe}$ is the projection of $\hat{\boldsymbol{\epsilon}}_{\rm probe}$ onto the plane perpendicular to $\hat{\mathbf{v}}$ and is given by

$$\mathbf{P}_{\rm probe}=\hat{\boldsymbol{\epsilon}}_{\rm probe}-\cos\Theta\hat{\mathbf{v}}. \tag{24}$$

The simulation of the time-of-flight profiles of photofragments characterized by $\beta=-0.6$, $\mathbf{a}_2^{(2)}(\perp)=+1$ and $s_2=1$ yields the profiles $\mathbf{B}_Z^Y[\mathbf{a}_2^{(2)}(\perp);t]$ and $\mathbf{B}_Y^Y[\mathbf{a}_2^{(2)}(\perp);t]$ (see Fig. 3). The notation used to describe the profiles $\mathbf{B}_G^F[\mathbf{a}_q^{(k)}(p);t]$ is as follows: the superscript F denotes the laboratory orientation of the photolysis polarization, and the subscript G denotes the laboratory orientation of the probe polarization; the basis function $\mathbf{B}_G^F[\mathbf{a}_q^{(k)}(p);t]$ exhibits a single $\mathbf{a}_q^{(k)}(p)$ parameter, and t indicates that $\mathbf{B}_G^F[\mathbf{a}_q^{(k)}(p);t]$ depends on the time of flight. The laboratory Z axis is defined to be parallel to the detection axis (such as the time-of-flight or Doppler axis). An indication of sign, such as $+Z$, denotes that the laser polarization is circularly polarized and is parallel to the Z axis; no sign indicates that the laser light is linearly polarized. For example, the basis function $\mathbf{B}_Z^{-Y}\{\mathrm{Im}[\mathbf{a}_1^{(2)}(\parallel,\perp)];t\}$ exhibits the parameter $\mathrm{Im}[\mathbf{a}_1^{(2)}(\parallel,\perp)]$ only, the photolysis polarization is circular and lies antiparallel to the Y axis, and the probe polarization is linear and lies along the Z axis. The profiles $\mathbf{B}_Z^X[\mathbf{a}_2^{(2)}(\perp);t]$ and $\mathbf{B}_X^X[\mathbf{a}_2^{(2)}(\perp);t]$ shown in Fig. 3 differ only in the laboratory orientation of the probe polarization direction; for the $\mathbf{B}_Z^X[\mathbf{a}_2^{(2)}(\perp);t]$ profile the probe polarization lies along the Z axis, and for the $\mathbf{B}_X^X[\mathbf{a}_2^{(2)}(\perp);t]$ the probe polarization lies along the X axis. Notice the large effects on the simulated signals caused by photofragment polarization.

The difference between two experimental profiles or basis functions that differ only in the direction of the probe polarization are known as anisotropic profiles or basis functions. These anisotropic basis functions are of key importance to the fitting of experimental signals. The anisotropic basis function $\mathbf{B}_{\rm aniso}^F[\mathbf{a}_q^{(k)}(p);t]$ is defined as $\mathbf{B}_Z^F[\mathbf{a}_q^{(k)}(p);t]-\mathbf{B}_X^F[\mathbf{a}_q^{(k)}(p);t]$ for linearly polarized probe light, and as $\mathbf{B}_{+G}^F[\mathbf{a}_q^{(k)}(p);t]-\mathbf{B}_{-G}^F[\mathbf{a}_q^{(k)}(p);t]$ for circularly polarized probe light. The important features of the anisotropic basis function $\mathbf{B}_{\rm aniso}^F[\mathbf{a}_q^{(k)}(p);t]$ is that it possesses a characteristic shape, and its magnitude is proportional to the $\mathbf{a}_q^{(k)}(p)$ parameter. Therefore, experimental anisotropic profiles $\mathbf{I}_{\rm aniso}^F$ can be fit with linear combinations of $\mathbf{B}_{\rm aniso}^F[\mathbf{a}_q^{(k)}(p);t]$ basis functions via linear least-squares fitting procedures to measure the $\mathbf{a}_q^{(k)}(p)$ directly:

$$\mathbf{I}_{\rm aniso}^F=\sum_{k,q,p}\mathbf{a}_q^{(k)}(p)c_{00}^F\mathbf{B}_{\rm aniso}^F[\mathbf{a}_q^{(k)}(p);t]. \tag{25}$$

The coefficient c_{00}^F in Eq. (25) is proportional to the population of the photofragments, and is obtained by a previous fit to a profile independent of photofragment polarization:

$$\mathbf{I}_{\rm iso}^F=c_{00}^F\mathbf{B}_{\rm iso}^F, \tag{26}$$

where the experimental profile $\mathbf{I}_{\rm iso}^F$ and the basis function $\mathbf{B}_{\rm iso}^F$ is independent of photofragment polarization [all $\mathbf{a}_q^{(k)}(p)$

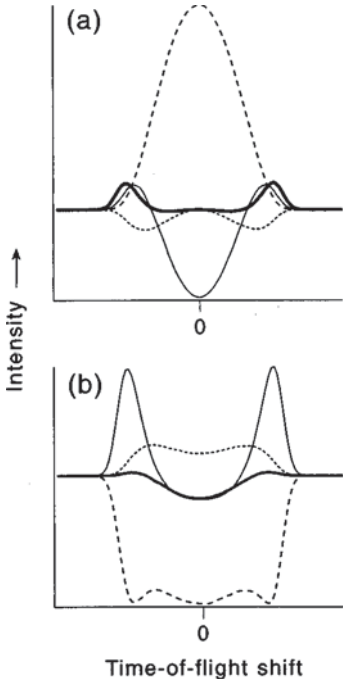

FIG. 4. (a) Four $k=2$ $\mathbf{B}^X_{\text{aniso}}[\mathbf{a}^{(2)}_q(p);t]$ profiles with the photolysis polarization parallel to the X axis and (b) four $k=2$ $\mathbf{B}^Z_{\text{aniso}}[\mathbf{a}^{(2)}_q(p);t]$ profiles with the photolysis polarization parallel to the Z axis. In both cases, the subscript aniso refers to the difference in profiles in which the probe polarization lies parallel to the Z and X axes. The profiles are given by: $\mathbf{B}^F_{\text{aniso}}[\mathbf{a}^{(2)}_0(\parallel);t]$ (thick solid line); $\mathbf{B}^F_{\text{aniso}}[\mathbf{a}^{(2)}_0(\perp);t]$ (thin solid line); $\mathbf{B}^F_{\text{aniso}}\{\text{Re}[\mathbf{a}^{(2)}_1(\parallel,\perp);t]\}$ (dotted line); and $\mathbf{B}^F_{\text{aniso}}[\mathbf{a}^{(2)}_2(\perp);t]$ (dashed line). The four profiles in (a) or the four profiles in (b) are not orthogonal. The four pairs of profiles, however, are orthogonal, therefore these geometries suffice to measure the four $k=2$ parameters independently.

$=0$ so that the laser-detection probability of Eq. (16) $I=1$]. The profiles $\mathbf{B}^F_{\text{iso}}$ and $\mathbf{I}^F_{\text{iso}}$ can be generated from the summation of profiles from various geometries.[13]

Figure 4(a) shows the four $k=2$ time-of-flight anisotropic basis functions $\mathbf{B}^X_{\text{aniso}}[\mathbf{a}^{(2)}_q(p);t]$, for which the photolysis polarization lies along the X axis. These four anisotropic basis functions are not linearly independent, so the anisotropic experimental profile $\mathbf{I}^X_{\text{aniso}}$ cannot be fit uniquely with these basis functions. Figure 4(b) shows the four $k=2$ time-of-flight anisotropic basis functions $\mathbf{B}^Z_{\text{aniso}}[\mathbf{a}^{(2)}_q(p);t]$, for which the photolysis polarization lies along the Z axis. Together, these four pairs of basis functions are now linearly independent, so that the experimental profiles $\mathbf{I}^X_{\text{aniso}}$ and $\mathbf{I}^Z_{\text{aniso}}$ can be fit simultaneously, using Eq. (25), to give the four values for the $\mathbf{a}^{(2)}_q(p)$. This technique was used in the measurement of the $\mathbf{a}^{(2)}_q(p)$ for ^{35}Cl and ^{37}Cl in the photodissociation of ICl,[10] and is also used similarly in the companion paper. The issue of linear dependence of the basis functions will be different in the case of ion imaging, as the images are of higher dimensionality and hence possess more information; in general, fewer geometries will be needed to ensure the linear dependence of the basis functions.

The $\text{Im}[\mathbf{a}^{(1)}_1(\parallel,\perp)]$ parameter is probed with the use of circularly polarized probe light. Figure 5 shows the anisotropic basis function $\mathbf{B}^{XZ}_{\text{aniso}}\{\text{Im}[\mathbf{a}^{(1)}_1(\parallel,\perp)];t\}$, which is the difference of basis functions in which the probe is varied

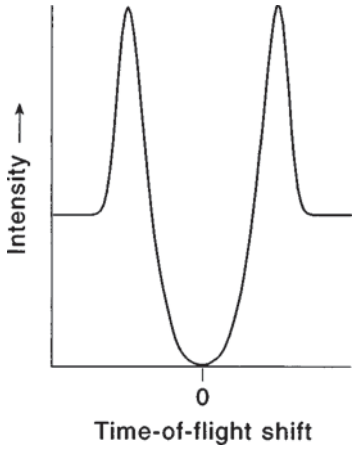

FIG. 5. $\mathbf{B}^{XZ}_{\text{aniso}}\{\text{Im}[\mathbf{a}^{(1)}_1(\parallel,\perp)];t\}$ profile for which the (linearly polarized) photolysis polarization lies at 45° to the Z axis in the X-Z plane. In this case, aniso refers to the difference in profiles in which the circularly polarized probe polarization lies parallel and antiparallel to the Y axis. These composite geometries are most sensitive to, and only sensitive to, orientation parameters with $q=1$.

between right and left circularly polarized with respect to the Y axis, and the photolysis polarization is linearly polarized along the XZ axis, an axis which lies at 45° to the Z axis in the X-Z plane.[13] The $\text{Im}[\mathbf{a}^{(1)}_1(\parallel,\perp)]$ parameter is sensitive to the shapes of the dissociative surfaces, as will be discussed in Sec. V.

In most experiments, the initial distribution of parent molecules is isotropic, and so the spatial distribution of the photofragments is described by Eq. (1). In some experiments, the parent molecules instead are prepared in the single state $|JKM\rangle$, where the quantization axis is given by the photolysis polarization. Then the spatial distribution is given by[19–21]

$$I(\theta_\epsilon)=[d^J_{KM}(\theta_\epsilon)]^2[1+\beta P_2(\cos\theta_\epsilon)], \tag{27}$$

where $d^J_{KM}(\theta)$ is a Wigner rotation matrix.[9] As discussed by Seideman,[22] Eq. (27) is only valid in the axial recoil limit. Note that when Eq. (27) is summed over all K, Eq. (1) is recovered, as expected. In the analysis of photodissociation experiments using aligned reagents, the modeling of the photofragment velocity distributions (described in Sec. II) will use Eq. (27) instead of Eq. (1). In the axial recoil limit [which is assumed for the results of this paper and for Eq. (27)], there is no geometrical information to be obtained by aligning the reagents. Therefore, in this limit, the only advantage of state-selecting the reagents is to control the internal energy of the reagents.

V. PHYSICAL INTERPRETATION

As discussed in the Introduction, other methods exist for the measurement and description of photofragment angular momentum distributions. The advantage of the present treatment of expressing the angular momentum distribution in the molecular frame is that it disentangles the factors that depend on the photofragment anisotropy (β) and on the angle between the photolysis polarization and recoil direction (θ_ϵ) from the molecular-frame distribution of angular momentum

vectors (Θ and Φ), which is described by the set of coefficients $\mathbf{a}_q^{(k)}(p)$. Once the $\mathbf{a}_q^{(k)}(p)$ are determined from a fit to laboratory observables (such as time-of-flight profiles) using appropriate basis functions (described in Sec. IV), the $\mathbf{a}_q^{(k)}(p)$ allow the photodissociation dynamics to be decomposed into fundamental components that make up a physical and intuitive picture: as discussed below, each $\mathbf{a}_q^{(k)}(p)$ parameter is sensitive to a different aspect of the photodissociation dynamics. In future work, we hope to connect the $\mathbf{a}_q^{(k)}(p)$ to Dixon's bipolar moment formalism expressed in the laboratory frame.

A. The $\mathbf{a}_0^{(k)}(p)$ parameters

Consider molecules that are in a definite quantum state, Ω, the projection of the total angular momentum onto the bond axis. Such molecules are cylindrically symmetric with respect to the recoil direction. The $\mathbf{a}_0^{(k)}(p)$ parameters describe photofragment angular momentum distributions that are also cylindrically symmetric about the recoil direction. Thus, dissociative states of the parent molecule of definite Ω should yield photofragments described by the $\mathbf{a}_0^{(k)}(p)$ parameters only. The $\mathbf{a}_q^{(k)}(p)$ parameters with $q \neq 0$ arise from the coherent excitation of two or more Ω states caused by the one-photon excitation process, as discussed below. The excited state of definite Ω correlates adiabatically to photofragments with predictable values of $\mathbf{a}_0^{(k)}(p)$. Thus, the deviation of the $\mathbf{a}_0^{(k)}(p)$ from their expected adiabatic values are a measure of the degree and nature of nonadiabatic effects of the photodissociation process. Examples involving the $\mathbf{a}_0^{(k)}(p)$ parameters are discussed in the companion paper.

The relationships between the density-matrix elements $\rho_{m'm}$ and the $\mathbf{A}_q^{(k)}$ are given by[8]

$$\rho_{m'm} = \sum_{k,q} (-1)^{J+q-m'} \frac{(2k+1)[J(J+1)]^{k/2}}{c(k)\langle J \| J^{(k)} \| J \rangle} \times \begin{pmatrix} J & k & J \\ -m & q & m' \end{pmatrix} \mathbf{A}_q^{(k)}, \tag{28}$$

$$\mathbf{A}_q^{(k)} = \frac{c(k)}{\langle Jm|\mathbf{J}^2|Jm\rangle^{k/2}} \sum_{m,m'} \rho_{m'm} \langle Jm|J_q^{(k)}|Jm'\rangle, \tag{29}$$

where the $\mathbf{A}_q^{(k)}$ are given, in general, by Eqs. (10)–(13); the $\mathbf{A}_0^{(k)}$ are equal to the $\mathbf{a}_0^{(k)}(\|)$ for $\beta = +2$, and equal to the $\mathbf{a}_0^{(k)}(\perp)$ for $\beta = -1$. The m-state probability distribution $p(J,m)$ along the recoil direction is given by ρ_{mm}; the $\mathbf{A}_0^{(k)}$ are expressed in terms of the ρ_{mm} only. For the dissociation of a molecule AB initially in state Ω, the photofragment m states must follow the relation $\Omega' = m_A + m_B$.

We illustrate these points through a simple example, which is also discussed in the following paper.[12] Consider the pure parallel ($\Delta\Omega = 0$) photodissociation of Cl_2 ($\Omega = 0$) to give $Cl\,^2P_{3/2}$ and $Cl\,^2P_{1/2}$ atoms, which we refer to as Cl and Cl*, respectively. The Cl* possesses the m states $\pm 1/2$, which are equally populated because parallel transitions cannot show orientation. The Cl possesses the m states $\pm 1/2$ and $\pm 3/2$, but since $\Omega' = m_{Cl} + m_{Cl}^* = 0$, only the $\pm 1/2$ states of the Cl atom are populated. The relationship between the m-state populations and the alignment parameter $\mathbf{a}_0^{(2)}(\|)$ can be derived from Eq. (29):

$$p(J = 3/2, |m| = 3/2) = \frac{1}{2}\left[1 + \frac{5}{4}\mathbf{a}_0^{(2)}(\|)\right], \tag{30}$$

$$p(J = 3/2, |m| = 1/2) = \frac{1}{2}\left[1 - \frac{5}{4}\mathbf{a}_0^{(2)}(\|)\right]. \tag{31}$$

Notice when $\mathbf{a}_0^{(2)}(\|) = +0.8$ only the $\pm 3/2$ states are populated, when $\mathbf{a}_0^{(2)}(\|) = -0.8$ only the $\pm 1/2$ states are populated, and when $\mathbf{a}_0^{(2)}(\|) = 0$ all states are equally populated. Therefore, in this example, the expected Cl atom alignment is described by $\mathbf{a}_0^{(2)}(\|) = -0.8$.

B. The $\mathbf{a}_1^{(k)}(\|,\perp)$ parameters

The $\mathbf{a}_1^{(k)}(\|,\perp)$ parameters arise solely from the interference of dissociating states associated with parallel and perpendicular transitions (for example, from the coherence of $\Omega = 0$ and $\Omega = \pm 1$ states). For a mixed transition, the transition dipole moment μ lies between the parallel and perpendicular axes of the molecule (see Fig. 2). Thus, the angular momentum of the excited state is separated into parallel and perpendicular components, which initially are in phase. Because the parallel and perpendicular dissociating pathways can be energetically different, an asymptotic phase difference, $\Delta\varphi$, can be introduced. This phase difference can be thought of as the phase difference in de Broglie waves associated with the two pathways, or as an energy-dependent quantum beat. The angular momentum can then be separated into components that are in phase (proportional to $\cos\Delta\varphi$), and components that are out of phase (proportional to $\sin\Delta\varphi$). The in-phase components correspond to linear polarization and are described by the $\mathrm{Re}[\mathbf{a}_1^{(2)}(\|,\perp)]$ parameter, and the out-of-phase components correspond to circular polarization and are described by the $\mathrm{Im}[\mathbf{a}_1^{(1)}(\|,\perp)]$ parameter. If multiple parallel and perpendicular states are present, then these parameters can be expressed in terms of the $\Delta\varphi$ as

$$\mathrm{Re}[\mathbf{a}_1^{(2)}(\|,\perp)] = \sum_{mn} c_{mn} \cos\Delta\varphi_{mn}, \tag{32}$$

$$\mathrm{Im}[\mathbf{a}_1^{(1)}(\|,\perp)] = \sum_{mn} c_{mn} \sin\Delta\varphi_{mn}, \tag{33}$$

where the subscript m labels the parallel states and n labels the perpendicular states, and the coefficient c_{mn} is the magnitude of the contribution from each interfering pair of states. Notice that for one parallel and one perpendicular state $\mathrm{Re}[\mathbf{a}_1^{(2)}(\|,\perp)]$ is proportional to $\cos\Delta\varphi$ and $\mathrm{Im}[\mathbf{a}_1^{(1)}(\|,\perp)]$ is proportional to $\sin\Delta\varphi$, so that both parameters contain similar information. However, the $\mathrm{Re}[\mathbf{a}_1^{(2)}(\|,\perp)]$ parameter, probed with linearly polarized probe light, must be detected simultaneously with the other three parameters with $k = 2$, whereas the $\mathrm{Im}[\mathbf{a}_1^{(1)}(\|,\perp)]$ parameter, probed with circularly polarized light, is the only $k = 1$ parameter that can be present (with linearly polarized photolysis light). Therefore, the detection of the $\mathrm{Im}[\mathbf{a}_1^{(1)}(\|,\perp)]$ parameter is much more convenient and sensitive for the measurement of $\Delta\varphi$.

The magnitude of $\Delta\varphi$ can be varied by changing the wavelength of the dissociating light. The observed variations in the $\mathbf{a}_1^{(k)}(\parallel,\perp)$ interference terms can then be used as a stringent test of the shapes of the dissociating surfaces. Variations in photofragment alignment as a function of the wavelength of dissociating light were observed in the photodissociation of H_2 and D_2.[23,24] These variations were observed as oscillations in the polarization of the Lyman-α fluorescence of the $H(2p)$ and $D(2p)$ photofragments formed from the coherent excitation of states accessed with both parallel and perpendicular transitions. The observed oscillations in the fluorescence polarization are caused by oscillations in the $\mathrm{Re}[\mathbf{a}_1^{(2)}(\parallel,\perp)]$ parameter only. Elegant examples of the measurement of the $\mathbf{a}_1^{(k)}(\parallel,\perp)$ interference terms have been performed in this laboratory for the photodissociation of ICl,[10,11] and are examined further in the companion paper.

C. The $\mathbf{a}_2^{(k)}$ parameters

The $\mathbf{a}_2^{(k)}(\perp)$ parameters are contributed from perpendicular transitions. For a perpendicular transition, μ is perpendicular to the bond of the parent molecule, and by definition lies along the x axis (see Fig. 2). Because of the $\mu\cdot\epsilon_{\mathrm{phot}}$ interaction, only the component of ϵ_{phot} along μ is absorbed. The one unit of angular momentum of the absorbed photon possesses no net projection ($m=0$) with respect to μ and the x axis. This breaking of cylindrical symmetry of the angular momentum of the excited parent molecule with respect to the bond axis can be expressed as a coherent superposition of states separated by $\Delta\Omega=2$ (such as a coherent superposition of the $\Omega'=+1$ and $\Omega'=-1$ excited states originating from the $\Omega=0$ ground state). This inequivalence of the x and y axes must be maintained in the photofragments. The $\mathbf{a}_2^{(k)}(\perp)$ parameters can be thought of as a measure of how the inequivalence of the x and y axes in the parent molecule is reflected in the photofragments. This point can be illustrated with three examples, called (a), (b), and (c).

A molecule AB with a ground states of $\Omega=0$ and no rotational angular momentum is excited via a perpendicular transition so that the $\Omega'=+1$ and $\Omega'=-1$ excited states are coherently excited. In example (a), the angular momentum of the photofragments $J_A=0$ and $J_B=1$, so that the angular momentum of the photon ($J_{\mathrm{photon}}=1$) is reflected entirely in J_B. Conservation of angular momentum constrains the spatial distribution of $\mathbf{J}_B$ to be identical to the spatial distribution of $\mathbf{J}_{\mathrm{photon}}$. This spatial distribution ($J=1$, $m=0$ with respect to the x axis) can be described by $\mathbf{A}_0^{(2)}=-1$ with respect to the x axis. Rotating to the bond axis gives $\mathbf{a}_0^{(2)}(\perp,B)=+0.5$ and $\mathbf{a}_2^{(2)}(\perp,B)=-\sqrt{3/8}$, so that in this example the value of the $\mathbf{a}_2^{(2)}(\perp,B)$ parameter is constrained. In example (b), the angular momentum of the photofragments $J_A=1/2$ and $J_B=1/2$, so that neither photofragment can possess nonzero values for parameters with $k\geqslant 2$ [$\mathbf{a}_0^{(2)}(\perp,B)=\mathbf{a}_2^{(2)}(\perp,B)=0$]. In this case, the spatial anisotropy of the parent molecule's angular momentum distribution is maintained in the correlation of $\mathbf{J}_A$ and $\mathbf{J}_B$; for example, m-state measurements with respect to the x axis will correlate $m_A=+1/2$ with $m_B=-1/2$, and $m_A=-1/2$ with $m_B=+1/2$ (so that $m_A+m_B=m=0$).

In example (c), the angular momentum of the photofragments $J_A=1/2$ and $J_B=3/2$. Unlike the previous examples, in this case the parent molecule angular momentum distribution can be expressed in $\mathbf{J}_A$ and $\mathbf{J}_B$ in more than one way. For example, the parent molecule anisotropy can be expressed entirely in $\mathbf{J}_B$ as in example (a), giving $\mathbf{a}_2^{(2)}(\perp,B)=-\sqrt{6}/5$ [while $\mathbf{a}_2^{(2)}(\perp,A)$ is always constrained to be zero]; also, the anisotropy can be expressed entirely in the correlation of $\mathbf{J}_A$ and $\mathbf{J}_B$ as in example (b), giving $\mathbf{a}_2^{(2)}(\perp,B)=0$. The manner in which the parent molecule angular momentum distribution is expressed in $\mathbf{J}_A$ and $\mathbf{J}_B$ depends on the symmetry of the excited state. Therefore, the determination of $\mathbf{a}_2^{(2)}(\perp,B)$ is a direct measurement of aspects of the symmetry of the dissociating states. Examples of the information that can be extracted from the $\mathbf{a}_2^{(2)}(\perp)$ parameter are given in the following paper.

ACKNOWLEDGMENTS

The authors thank O. S. Vasyutinskii for useful discussions. This work has been supported by the National Science Foundation under Grant No. CHE-93-22690.

APPENDIX A: TRANSITION DIPOLE MATRIX ELEMENTS

Siebbeles *et al.*[6] studied quantum mechanically the molecular photodissociation yielding two photofragments, of which one carries an angular momentum j and the other carries no angular momentum. The dependence of the photofragment polarization was described in terms of the dynamical functions, $f_K(q,q')$, which in turn were expressed in terms of the transition dipole matrix elements, $M_{j\Omega_i\Omega}$:

$$f_K(q,q')=\sum_{\Omega_i}(-1)^{j+\Omega_i-q}\begin{pmatrix} j & j & K \\ -\Omega & \Omega' & q'-q\end{pmatrix}\times M_{j\Omega_i\Omega}(M_{j\Omega_i\Omega})^*. \tag{A1}$$

The $\mathbf{a}_q^{(k)}(p)$ are expressed here in terms of the $f_K(q,q')$, and hence, using Eq. (A1), can ultimately be expressed in terms of the transition dipole matrix elements:

$$\mathbf{a}_0^{(1)}(\perp)=3(2j+1)\frac{f_1(1,1)}{f_0(1,1)}, \tag{A2}$$

$$\mathbf{a}_1^{(1)}(\parallel,\perp)=3(2j+1)\frac{f_1(1,0)}{f_0(0,0)+2f_0(1,1)}, \tag{A3}$$

$$\mathbf{a}_0^{(2)}(\parallel)=\sqrt{5(2j+1)}N(j)\frac{f_2(0,0)}{f_0(0,0)}, \tag{A4}$$

$$\mathbf{a}_0^{(2)}(\perp)=\sqrt{5(2j+1)}N(j)\frac{f_2(1,1)}{f_0(1,1)}, \tag{A5}$$

$$\mathbf{a}_1^{(2)}(\parallel,\perp)=3\sqrt{15(2j+1)}N(j)\frac{f_2(1,0)}{f_0(0,0)+2f_0(1,1)}, \tag{A6}$$

$$\mathbf{a}_2^{(2)}(\perp)=\frac{\sqrt{30(2j+1)}}{8}N(j)\frac{f_2(1,-1)}{f_0(1,1)}, \tag{A7}$$

where

$$N(j)=\left[\frac{(2j-1)(2j+1)(2j+3)}{5j(j+1)}\right]^{1/2}. \tag{A8}$$

APPENDIX B: CIRCULARLY POLARIZED PHOTOLYSIS LIGHT

The use of circularly polarized photolysis light reduces further the symmetry of the problem, such that the photofragment polarization can possess the polarization parameters (with $k\leqslant 2$) $\mathbf{a}_0^{(1)}(\perp)$, $\mathrm{Re}[\mathbf{a}_1^{(1)}(\parallel,\perp)]$, and $\mathrm{Im}[\mathbf{a}_1^{(2)}(\parallel,\perp)]$. The molecular-frame axes require different definitions. The z axis lies either parallel or antiparallel to the recoil direction $\hat{\mathbf{v}}$, so that it lies parallel to the projection of $\boldsymbol{\epsilon}_{\mathrm{phot}}$ along $\hat{\mathbf{v}}$. The y axis is then given by $\hat{y}=\hat{\boldsymbol{\epsilon}}_{\mathrm{phot}}\times\hat{z}$. Using circularly polarized photolysis light, the relative detection probability of the photofragments is given by

$$\begin{aligned} I[\Theta,\Phi,\theta_\epsilon,\beta,\mathbf{a}_q^{(k)}(p)] = 1+(s_1\{&(1-\beta/2)\sin^2\theta_\epsilon\cos\Theta\,\mathbf{a}_0^{(1)}(\perp)-\sin\theta_\epsilon\cos\theta_\epsilon\,\mathrm{Re}[\mathbf{a}_1^{(1)}(\parallel,\perp)](1/\sqrt{2})\\ &\times\sin\Theta\cos\Phi-\sin\theta_\epsilon\cos\theta_\epsilon\,\mathrm{Im}[\mathbf{a}_1^{(1)}(\parallel,\perp)](1/\sqrt{2})\sin\Theta\sin\Phi\}+s_2\{(1+\beta)\cos^2\theta_\epsilon\mathbf{a}_0^{(2)}\\ &\times(\parallel)P_2(\cos\Theta)+(1-\beta/2)\sin^2\theta_\epsilon\,\mathbf{a}_0^{(2)}(\perp)P_2(\cos\Theta)-\sin\theta_\epsilon\cos\theta_\epsilon\,\mathrm{Re}[\mathbf{a}_1^{(2)}(\parallel,\perp)]\sqrt{3/8}\\ &\times\sin 2\Theta\cos\Phi-\sin\theta_\epsilon\cos\theta_\epsilon\,\mathrm{Im}[\mathbf{a}_1^{(2)}(\parallel,\perp)]\sqrt{3/8}\sin 2\Theta\sin\Phi-(1-\beta/2)\sin^2\theta_\epsilon\mathbf{a}_2^{(2)}\\ &\times(\perp)\sqrt{3/8}\sin^2\Theta\cos 2\Phi\})/[1+\beta P_2(\cos\theta_\epsilon)]. \end{aligned} \tag{B1}$$

Other than the addition of the new parameters, notice that, compared to Eq. (16), the parameters with $q\neq 0$ in Eq. (B1) are multiplied by -0.5. The sensitivity of the polarization parameters to the polarization of the photolysis and probe light is summarized in Table I. The definition of the angles in Eq. (B1) become seemingly ambiguous when linearly polarized probe or photolysis light are used, as linearly polarized light is represented as a double-headed arrow (see Fig. 2). However, Eq. (B1) reflects the properties summarized in Table I: for the parameters that are sensitive to linearly polarized light, the choice of either head of the double-headed arrow yields the same answer. A more detailed discussion of the parameters arising from the use of circularly polarized photolysis light in conjunction with relevant experimental results is deferred to a future publication.[25]

TABLE I. Experimental sensitivity to the $k\leqslant 2$ polarization parameters as a function of the nature of the polarization of the photolysis and probe light for a single excitation-detection geometry. Note that if two excitation-detection geometries with linearly polarized probe light are subtracted, then the difference signal is sensitive to parameters of even k, whereas the difference signal for circularly polarized probe light is sensitive to parameters of odd k.

		Photolysis polarization	
		Linear	Circular
Probe polarization	linear	$\mathbf{a}_0^{(2)}(\parallel)$, $\mathbf{a}_0^{(2)}(\perp)$ $\mathrm{Re}[\mathbf{a}_1^{(2)}(\parallel,\perp)]$ $\mathbf{a}_2^{(2)}(\perp)$	$\mathbf{a}_0^{(2)}(\parallel)$, $\mathbf{a}_0^{(2)}(\perp)$ $\mathrm{Re}[\mathbf{a}_1^{(2)}(\parallel,\perp)]$, $\mathrm{Im}[\mathbf{a}_1^{(2)}(\parallel,\perp)]$ $\mathbf{a}_2^{(2)}(\perp)$
	circular	$\mathrm{Im}[\mathbf{a}_1^{(1)}(\parallel,\perp)]$ $\mathbf{a}_0^{(2)}(\parallel)$, $\mathbf{a}_0^{(2)}(\perp)$ $\mathrm{Re}[\mathbf{a}_1^{(2)}(\parallel,\perp)]$ $\mathbf{a}_2^{(2)}(\perp)$	$\mathbf{a}_0^{(1)}(\perp)$ $\mathrm{Re}[\mathbf{a}_1^{(1)}(\parallel,\perp)]$, $\mathrm{Im}[\mathbf{a}_1^{(1)}(\parallel,\perp)]$ $\mathbf{a}_0^{(2)}(\parallel)$, $\mathbf{a}_0^{(2)}(\perp)$ $\mathrm{Re}[\mathbf{a}_1^{(2)}(\parallel,\perp)]$, $\mathrm{Im}[\mathbf{a}_1^{(2)}(\parallel,\perp)]$ $\mathbf{a}_2^{(2)}(\perp)$

[1] R. N. Zare and D. R. Herschbach, Proc. IEEE **51**, 173 (1963).
[2] R. N. Dixon, J. Chem. Phys. **85**, 1866 (1986).
[3] D. A. Case, G. M. McClelland, and D. R. Herschbach, Mol. Phys. **35**, 541 (1978).
[4] G. E. Hall and P. L. Houston, Annu. Rev. Phys. Chem. **40**, 375 (1989).
[5] O. S. Vasyutinskii, Opt. Spektrosk. **54**, 524 (1983).
[6] L. D. A. Siebbeles, M. Glass-Maujean, O. S. Vasyutinskii, J. A. Beswick, and O. Roncero, J. Chem. Phys. **100**, 3610 (1994).
[7] K.-M. Chen and C.-C. Pei, J. Chem. Phys. **109**, 6647 (1998).
[8] A. J. Orr-Ewing and R. N. Zare, Annu. Rev. Phys. Chem. **45**, 315 (1994).
[9] R. N. Zare, *Angular Momentum, Understanding Spatial Aspects in Chemistry and Physics* (Wiley–Interscience, New York, 1988).
[10] T. P. Rakitzis, S. A. Kandel, and R. N. Zare, J. Chem. Phys. **108**, 8291 (1998).
[11] T. P. Rakitzis, S. A. Kandel, A. J. Alexander, Z.-H. Kim, and R. N. Zare, Science **281**, 1346 (1998).
[12] T. P. Rakitzis, S. A. Kandel, A. J. Alexander, Z. H. Kim, and R. N. Zare, J. Chem. Phys. **110**, 3351 (1999), following paper.
[13] T. P. Rakitzis, S. A. Kandel, and R. N. Zare, J. Chem. Phys. **107**, 9382 (1997).
[14] D. V. Kupriyanov and O. S. Vasyutinskii, Chem. Phys. **171**, 25 (1993).
[15] A. C. Kummel, G. O. Sitz, and R. N. Zare, J. Chem. Phys. **85**, 6874 (1986).
[16] A. C. Kummel, G. O. Sitz, and R. N. Zare, J. Chem. Phys. **88**, 6707 (1988).
[17] A. J. Orr-Ewing, W. R. Simpson, T. P. Rakitzis, and R. N. Zare, Isr. J. Chem. **34**, 95 (1994).
[18] S. A. Kandel, T. P. Rakitzis, T. Lev-On, and R. N. Zare, J. Chem. Phys. **105**, 7550 (1996).
[19] S. E. Choi and R. B. Bernstein, J. Chem. Phys. **85**, 150 (1986).
[20] R. N. Zare, Chem. Phys. Lett. **156**, 1 (1989).
[21] J. A. Beswick, Chem. Phys. **42**, 191 (1979).
[22] T. Seideman, Chem. Phys. Lett. **253**, 279 (1996).
[23] E. Flemming, G. Reichardt, H. Schmoranzer, and O. Wilhelmi, Phys. Lett. A **192**, 52 (1994).
[24] E. Flemming, O. Wilhelmi, H. Schmoranzer, and M. Glass-Maujean, J. Chem. Phys. **103**, 4090 (1995).
[25] T. P. Rakitzis, S. A. Kandel, A. J. Alexander, and R. N. Zare (unpublished).